Virulence

ISSN: (Print) (Online) Journal homepage: www.tandfonline.com/journals/kvir20

The response to desiccation in *Acinetobacter baumannii*

Massimiliano Lucidi, Giulia Capecchi, Cinzia Spagnoli, Arianna Basile, Irene Artuso, Luca Persichetti, Elisa Fardelli, Giovanni Capellini, Daniela Visaggio, Francesco Imperi, Giordano Rampioni, Livia Leoni & Paolo Visca

To cite this article: Massimiliano Lucidi, Giulia Capecchi, Cinzia Spagnoli, Arianna Basile, Irene Artuso, Luca Persichetti, Elisa Fardelli, Giovanni Capellini, Daniela Visaggio, Francesco Imperi, Giordano Rampioni, Livia Leoni & Paolo Visca (2025) The response to desiccation in *Acinetobacter baumannii*, Virulence, 16:1, 2490209, DOI: 10.1080/21505594.2025.2490209

To link to this article: https://doi.org/10.1080/21505594.2025.2490209

Published online: 12 Apr 2025.

VIRULENCE
2025, VOL. 16, NO. 1, 2490209
https://doi.org/10.1080/21505594.2025.2490209

Taylor & Francis
Taylor & Francis Group

RESEARCH ARTICLE

OPEN ACCESS Check for updates

The response to desiccation in *Acinetobacter baumannii*

Massimiliano Lucidi [a,b*], Giulia Capecchi [a*], Cinzia Spagnoli[a], Arianna Basile[a], Irene Artuso[a], Luca Persichetti [a], Elisa Fardelli [a], Giovanni Capellini [a], Daniela Visaggio [a,b,c], Francesco Imperi[a,b,c], Giordano Rampioni [a,c], Livia Leoni [a], and Paolo Visca [a,b,c]

[a]Department of Science, Roma Tre University, Rome, Italy; [b]NBFC, National Biodiversity Future Center, Palermo, Italy; [c]Santa Lucia Foundation IRCCS, Rome, Italy

ABSTRACT

The long-term resistance to desiccation on abiotic surfaces is a key determinant of the adaptive success of *Acinetobacter baumannii* as a healthcare-associated bacterial pathogen. Here, the cellular and molecular mechanisms enabling *A. baumannii* to resist desiccation and persist on abiotic surfaces were investigated. Experiments were set up to mimic the *A. baumannii* response to air-drying that would occur when bacterial cells contaminate fomites in hospitals. Resistance to desiccation and transition to the "viable but nonculturable" (VBNC) state were determined in the laboratory-adapted strain ATCC 19606^T and the epidemic strain ACICU. Culturability, membrane integrity, metabolic activity, virulence, and gene expression profile were compared between the two strains at different stages of desiccation. Upon desiccation, ATCC 19606^T and ACICU cells lose culturability and membrane integrity, lower their metabolism, and enter the VBNC state. However, desiccated *A. baumannii* cells fully recover culturability and virulence in an insect infection model following rehydration in physiological buffers or human biological fluids. Transcriptome and chemical analyses of *A. baumannii* cells during desiccation unveiled the production of protective metabolites (L-cysteine and L-glutamate) and decreased energetic metabolism consequent to activation of the glyoxylate shunt (GS) pathway, as confirmed by reduced resuscitation efficiency of *aceA* mutants, lacking the key enzyme of the GS pathway. VBNC cell formation and extensive metabolic reprogramming provide a biological basis for the response of *A. baumannii* to desiccation, with implications on environmental control measures aimed at preventing the transmission of *A. baumannii* infection in hospitals.

ARTICLE HISTORY
Received 26 September 2024
Revised 10 February 2025
Accepted 2 April 2025

KEYWORDS
AceA; glyoxylate shunt; membrane permeability; resuscitation; VBNC

Introduction

Acinetobacter baumannii is a frequent colonizer of hospitalized patients and causes severe disease, including ventilator-associated pneumonia, urinary tract infection, bacteraemia, meningitis, and skin or soft tissue infections, particularly in intensive care unit (ICU) patients [1–3]. Recently, the incidence of *A. baumannii* infections increased by more than 110% due to the SARS-CoV-2 pandemic, often resulting in lethal co-infections [4,5]. Therefore, *A. baumannii* infections are now considered a worrisome problem on a global scale due to the healthcare burden, increasing trend of antibiotic resistance, and high transmissibility among patients [2]. Contamination of the environment has been documented in outbreaks for which information about environmental sampling was reported [6]. Asymptomatic *A. baumannii* carriage on the skin, in the pharynx, and the gastrointestinal tract has frequently been linked to significant contamination in the near surroundings of patients (reviewed by Dijkshoorn *et al.*, 2007 [1]). Transmission of this pathogen is facilitated by hospital personnel, airflow, shared equipment, plumbing systems, and other fomites that constitute an *A. baumannii* reservoir of infections [7]. Managing outbreaks of *A. baumannii* sometimes necessitate ward closure and impose decontamination interventions or modifications to infrastructure which cause clinical, financial, and logistical burdens [1,2].

The striking ability to endure long-term desiccation is a major obstacle to *A. baumannii* eradication from the hospital environment, making this pathogen a model organism to investigate the effects of air-desiccation and osmostress on Gram-negative bacteria [8]. The ability of *A. baumannii* to survive water loss has so far been ascribed to the biosynthesis of compatible solutes, namely L-glutamate, D-mannitol, and trehalose, which act as osmoprotectants to prevent

CONTACT Massimiliano Lucidi massimiliano.lucidi@uniroma3.it; Paolo Visca paolo.visca@uniroma3.it
*These authors contributed equally to this work: Massimiliano Lucidi, Giulia Capecchi.

macromolecular damages caused by dehydration (reviewed by Zeidler and Müller [8]), and the expression of the DtpA and DtpB hydrophilins, which act as molecular chaperones to prevent desiccation-induced protein denaturation [9]. It has also been demonstrated that *A. baumannii* enters a state of metabolic quiescence induced by dehydration, known as the "viable but not culturable" (VBNC) state [10]. Since culture-based procedures for assessing bacterial contamination in the hospital environment rely on the assumption that one viable cell gives rise to one colony on a solid medium [11], transition to the VBNC state would reduce bacterial detection given that VBNC cells, by definition, do not grow on solid media normally used for environmental control [12]. Indeed, the notion that the most successful *A. baumannii* clinical strains are endowed with higher desiccation resistance compared to laboratory-adapted strains is based on their ability to form colonies after desiccation [13,14]. However, the existence of a VBNC state challenges the paradigm "one viable cell=one colony" in assessing bacterial viability, posing the need to consider VBNC cells as an integral, still-alive component of the entire population challenged with the desiccation stress. Here, we elucidate the cellular and molecular mechanisms governing the transition to the desiccation-induced VBNC state in two *A. baumannii* prototypic strains endowed with different levels of desiccation resistance and discuss the impact of VBNC cell formation on environmental surveillance and hospital infection control.

Results

A. baumannii *culturability during desiccation*

Preliminarily, we set the culture conditions ensuring 100% culturability of *A. baumannii* cells for desiccation experiments. To this aim, culturability [expressed as colony-forming unit (CFU) values], cell density (OD_{600}), and membrane integrity (the principal viability marker) were compared between the type strain ATCC 19606^T and the epidemic strain ACICU taken at different times during growth in Luria Bertani (LB) medium (Figure S1). Although the CFU/OD_{600} values did not change during 24-h growth, membrane damage became detectable after 14 h (Figure S1). Hence, to evaluate the clonogenic potential of *A. baumannii* undergoing desiccation, 6-h cultures of ATCC 19606^T and ACICU, showing maximum culturability and membrane integrity, were desiccated on a glass surface for up to 8 weeks or maintained in water as control (Figure 1a). Desiccation caused a progressive reduction of culturability of both strains, with ACICU retaining its colony-forming ability 6 weeks longer than ATCC 19606^T. Storage in water for up to 4 weeks did not affect *A. baumannii* culturability, whereas a moderate (<1 Log) decrease in CFU counts was observed after 8 weeks (Figure 1b).

A. baumannii *transition to the VBNC state during desiccation*

To study the clonogenic potential of desiccated cells at the single-cell level, the pVRL1*gfp* plasmid directing constitutive expression of the green fluorescent protein (GFP [15]) was introduced in both *A. baumannii* ATCC 19606^T and ACICU strains. GFP-expressing cells desiccated for 0, 6, and 24 h were overlaid with a pad of LB soft (0.5% agarose) medium supplemented with a subinhibitory concentration of propidium iodide (PI, 60 µM; Figure S2) to label membrane-damaged cells, and bacterial replication was continuously monitored for 4 h by time-lapse confocal microscopy. Four distinct *A. baumannii* sub-populations were found to co-exist after desiccation, hereafter classified as type I to type IV cells (Figure 1c): type I, clonogenic green-fluorescent cells; type II, non-clonogenic green-fluorescent cells; type III, non-clonogenic cells, which lose green fluorescence and adsorb PI over time; type IV, non-clonogenic red-fluorescent cells (Figure 1d and Supplementary videos 1–2). The inability to replicate despite membrane integrity, as proven by the cytoplasmic retention of GFP (27-kDa protein; *ca.* 4 × 3 nm size [16]) and PI exclusion, conforms type II cells to typical VBNC cells [12]. Conversely, type III and IV cells are endowed with typical features of dead cells due to PI intake, GFP release, and loss of clonogenicity. Quantification of these subpopulations revealed that the number of type II cells and, to a lesser extent, type IV cells increased during desiccation for both strains, denoting a progressive switch to the VBNC and dead states, respectively (Figure 1e). Moreover, the percentage of type II (typical VBNC) cells after 6- and 24-h desiccation was higher in ATCC 19606^T than in ACICU (Figure 1e). The decrease of green fluorescence emission by type III and IV cells should be attributed to GFP leakage from damaged cells, since GFP levels in the supernatants increased proportionally to the desiccation time and loss of cell-associated fluorescence (Figure S3). Plasmid loss was excluded since nearly 100% of the population of both strains maintained the pVRL1*gfp* plasmid (Figure S4).

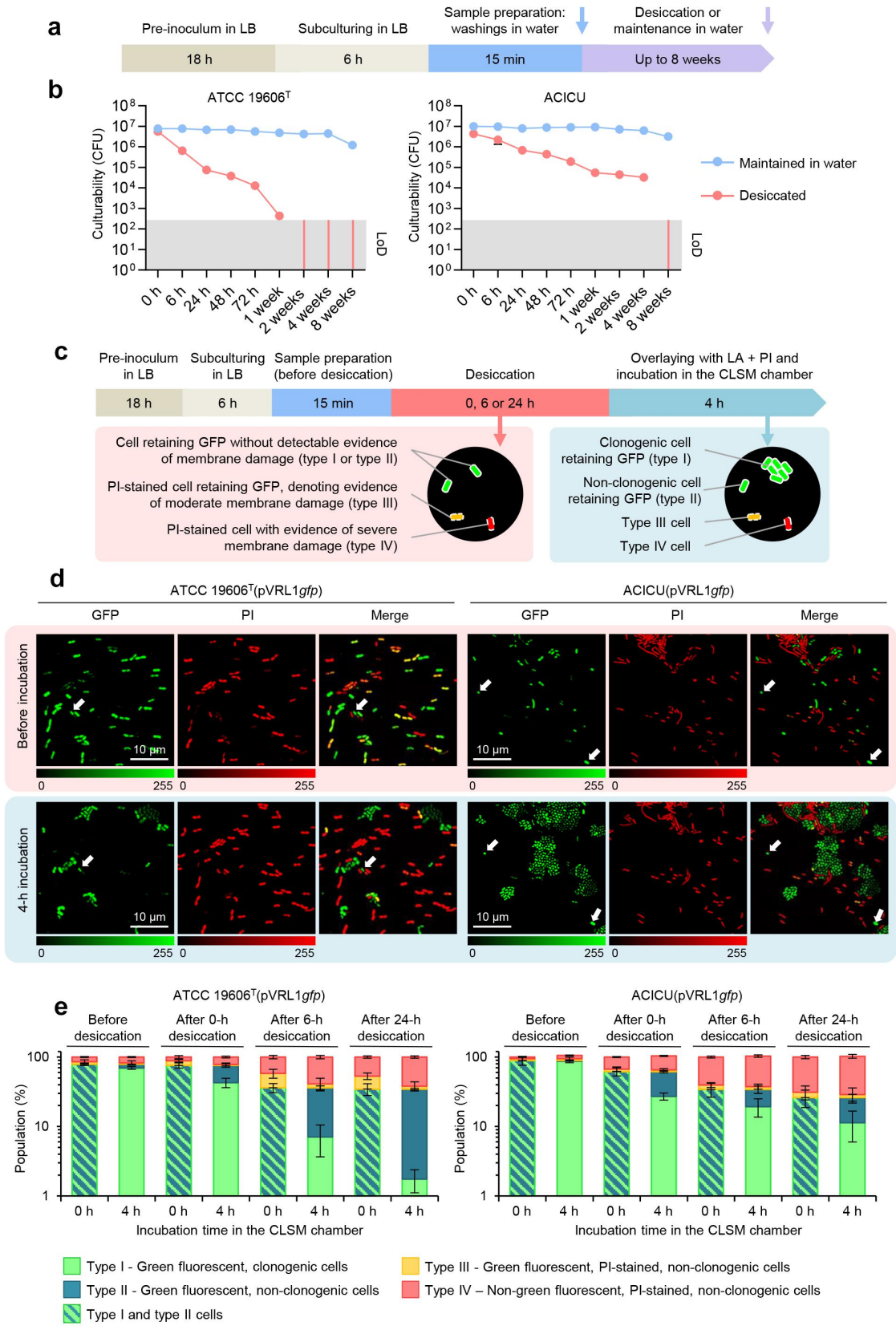

Figure 1. Resistance to desiccation and entry of *A. baumannii* cells in the non-clonogenic state after desiccation. (a) Experimental timeline of the desiccation resistance assay. Colored arrows indicate the sampling times for CFU counts; cyan, before desiccation; purple, after desiccation. (b) Clonogenic ability (CFU counts) of ATCC 19606^{T} and ACICU cells kept in water or desiccated for up to 8 weeks. The grey area indicates the lower detection limit (LoD) of CFU counts, corresponding to 4×10^{2} CFU, with red segments

Factors affecting the resuscitation of VBNC A. baumannii cells

Resuscitation is defined as the regain of clonogenicity (*i.e.*, the ability to generate a colony from a single cell on a solid medium) by stress-induced VBNC cells, and it can occur by removing the stressing factor [12]. As previously demonstrated, ATCC 19606^T cells can be resuscitated after osmotic stress and dehydration, although with a low efficiency [10]. Therefore, the resuscitation of desiccated *A. baumannii* cells was investigated by measuring their culturability and membrane integrity after 24-h incubation at 37°C in M9 basal salt solution (M9SS $Mg^{2+}Ca^{2+}$), a mineral medium containing Mg^{2+} and Ca^{2+} ions but devoid of any carbon source (Figure 2a). Interestingly, a complete regain of clonogenicity was observed for both ATCC 19606^T and ACICU strains after 24-h incubation in M9SS $Mg^{2+}Ca^{2+}$, irrespective of the initial composition of the population (Figure 2b). Resuscitation was associated with complete recovery of membrane integrity, as inferred from PI exclusion (Figure 2c). This indicates that not only the typical VBNC population (type II) but also the populations composed of apparently dead cells, characterized by severely damaged membranes and leakage of intracellular GFP (type III and IV; Figure 1c), can be resuscitated, and therefore should be considered in a VBNC-like state. Low temperature and absence of membrane-stabilizing cations dramatically affected resuscitation, since culturability and regain of membrane integrity were reduced by incubation at 4°C and depletion of Mg^{2+} and Ca^{2+} ions [M9SS, phosphate-buffered saline (PBS)] (Figure S5). Under these sub-optimal conditions, the resuscitation efficiency greatly differed between ATCC 19606^T and ACICU, the latter being less sensitive to Mg^{2+} and Ca^{2+} depletion and low temperature (Figure S5). Thus, the epidemic strain ACICU remains culturable during longer desiccation periods than ATCC 19606^T (Figure 1b) and regains culturability and membrane integrity under sub-optimal resuscitation conditions (Figure S5). Intriguingly, resuscitation kinetic assays revealed that 12-h incubation in M9SS $Mg^{2+}Ca^{2+}$ at 37°C was sufficient to ensure complete recovery of culturability and membrane integrity of both the *A. baumannii* strains (Figure S6).

We also used vancomycin (Van), a glycopeptide antibiotic excluded by the *A. baumannii* outer membrane but capable of penetrating it when the membrane is damaged [17], to probe membrane permeability of cells before and after desiccation, and after resuscitation. The minimal inhibitory concentration (MIC) of Van was similarly high (256 mg/L) for ATCC 19606^T and ACICU in all the test conditions (Figure S7). However, time-killing assays revealed that desiccated cells were more rapidly killed by inhibitory Van concentrations (512 mg/L; 2 × MIC) than cells before desiccation or after resuscitation, confirming that desiccation perturbs the outer membrane and facilitates Van penetration (Figure S7).

Since both *A. baumannii* strains were able to resuscitate after desiccation, we wondered if VBNC formation and resuscitation are common features of other members of the *Acinetobacter* genus. Therefore, four additional *A. baumannii* strains (ATCC 17978, AB5075, RUH 5875, and AYE) and representative strains belonging to other species of the genus (*Acinetobacter nosocomialis*, *Acinetobacter pittii*, *Acinetobacter baylyi*, *Acinetobacter seifertii*, and *Acinetobacter lactucae*) were desiccated, and their ability to resuscitate was assessed. Albeit with different resuscitation efficiencies, all *A. baumannii* strains and *Acinetobacter* species entered the VBNC state after desiccation and recovered culturability upon incubation in M9SS $Mg^{2+}Ca^{2+}$. Notably, *A. baumannii* AB5075 and *A. pittii* showed the highest resistance to desiccation (Figure S8).

Structural and functional modifications of desiccated A. baumannii cells

To better characterize the transitions in and out of the VBNC state, desiccated and resuscitated cells of

representing all CFU values below the LoD. Data are the mean±standard deviation (SD; error bars) of three independent experiments. (c) Graphical representation of the confocal laser-scanning microscopy (CLSM) imaging experiment. ATCC 19606^T (pVRL1*gfp*) and ACICU(pVRL1*gfp*) cells were desiccated on a glass coverslip, covered with a pad of LB 0.5% agarose supplemented with 60 μM PI, and observed in a CLSM incubation chamber. Bacterial subpopulations (type I-IV) were quantified before and after 4-h incubation at 37°C. (d) Representative time-lapse CLSM micrographs of cells before and after 4-h incubation at 37°C. White arrows indicate type II cells. Green and red scales denote pixel intensity. (e) Percentages of cells belonging to type I, II, III, and IV subpopulations, calculated before (0 h) and after (4 h) incubation in the CLSM chamber ($n > 6{,}500$ for each sample). The distinction between type I and II cells is based on bacterial replication after 4-h incubation at 37°C.

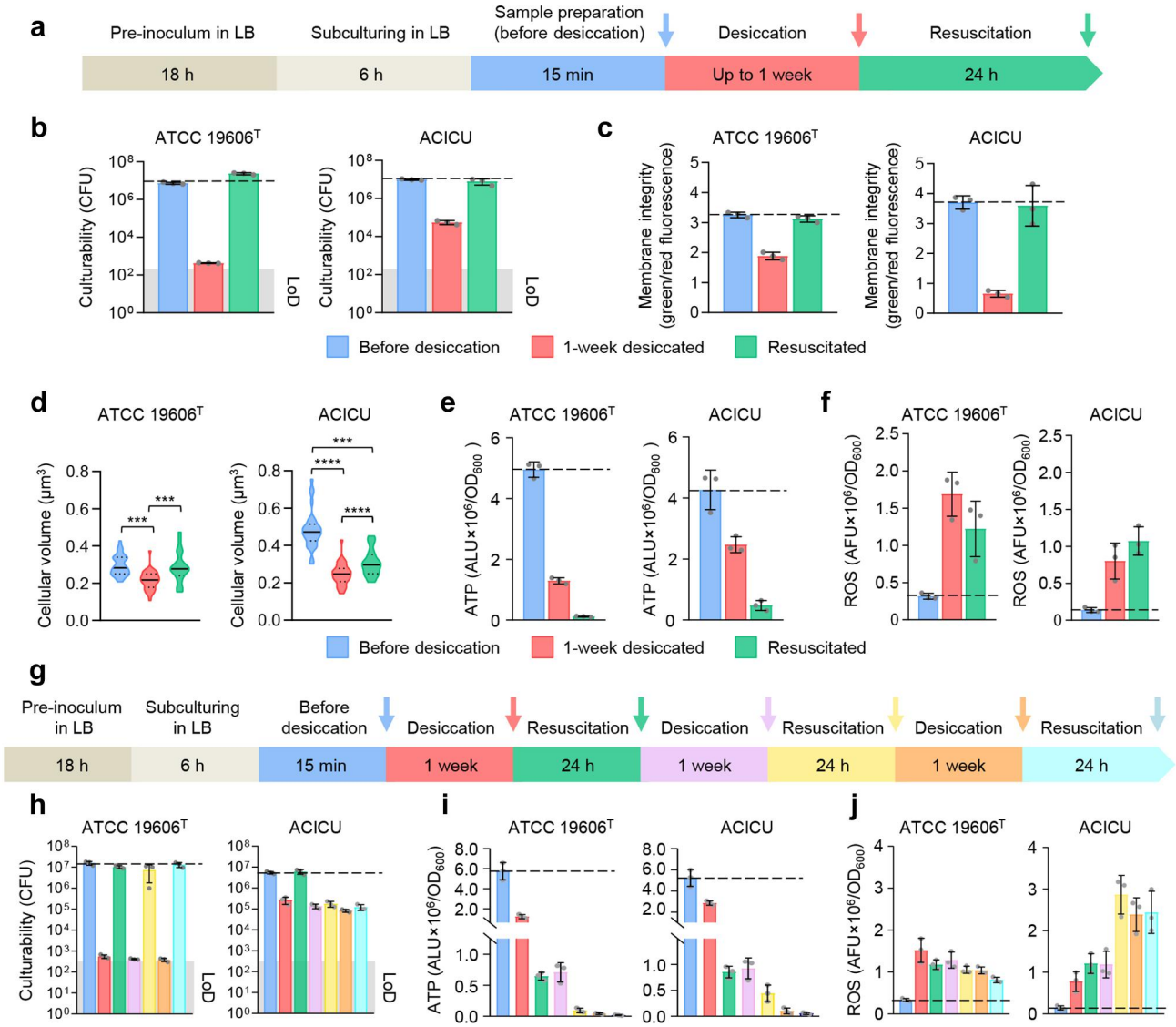

Figure 2. Formation of VBNC cells upon desiccation and analysis of structural and functional alterations occurring during *A. baumannii* desiccation and resuscitation. (a) Timeline of the resuscitation assay. ATCC 19606^T and ACICU cells were air-dried for 1 week. After desiccation, cells were suspended in M9SS $Mg^{2+}Ca^{2+}$ and incubated at 37°C for 24 h under shaking (resuscitation). Colored arrows indicate the sampling times for CFU counts; cyan, before desiccation; red, after desiccation; green, after resuscitation. (b) Culturability (expressed as CFU) of cells before desiccation, after desiccation, and after resuscitation. (c) Membrane integrity expressed as the ratio between green (SYTO 9) and red (PI) fluorescence emissions. (d) Cell volume before desiccation, after 1-week desiccation, and after resuscitation, as determined by AFM imaging of 30 cells of ATCC 19606^T and ACICU. The median (filled lines) and interquartile ranges (dashed lines) are shown. ATP (e) and ROS (f) levels in ATCC 19606^T and ACICU cells before desiccation, after desiccation, and after resuscitation. (g) Timeline of the resuscitation assays performed after three rounds of desiccation. Colored arrows indicate the sampling times for CFU counts (h), ATP levels (i), and ROS content (j). Color codes of histograms in (h,i,j) are those used in the experimental timeline (g). The grey area in (b) and (h) indicates the LoD of CFU counts (4×10^2 CFU). Dashed lines in histograms (b,c,e,f,h,i,j) indicate the pre-desiccation values. Data are the mean±SD (error bars) of three independent experiments. Statistical significance was determined by the unpaired *t*-test (***$p < 0.001$; ****$p < 0.0001$).

ATCC 19606^T and ACICU were analysed at both morphological and metabolic levels. Atomic force microscopy (AFM) measurements revealed that desiccation results in a significant loss of cellular volume, consequent to water evaporation, more evident in ACICU than in ATCC 19606^T. Upon resuscitation, desiccated ATCC 19606^T cells fully recovered their pre-desiccation volume, whereas ACICU did not. However, ATCC 19606^T and ACICU showed nearly identical cellular volumes after desiccation and after resuscitation (Figure 2d, Figure S9).

Dehydration causes energy consumption and the generation of reactive oxygen species (ROS) due to membrane damage and respiratory chain misfunction [18]. Quantitative ATP and ROS content estimation demonstrated that ATCC 19606^T and ACICU suffer from severe ATP depletion and ROS production during desiccation (Figure 2e-f). During resuscitation, intracellular ATP was further consumed (Figure 2e), while ROS production continued (Figure 2f), denoting that resuscitation is an energy-demanding process laden with oxidative stress.

Since both desiccation and resuscitation are energy-demanding processes, we wondered whether *A. baumannii* could endure multiple rounds of desiccation and resuscitation in the absence of carbon and energy source supply (Figure 2g). ATCC 19606^T recovered full culturability across 3 rounds of desiccation and resuscitation, while ACICU failed to resuscitate after the first round, despite its higher tolerance to multiple rounds of desiccation (Figure 2h). Both strains experienced a progressive decline in ATP content during three rounds of desiccation and resuscitation (Figure 2i). Different from ATCC 19606^T, ROS levels progressively increased in ACICU during multiple rounds of desiccation and resuscitation (Figure 2j), in line with reduced culturability.

Resuscitation in biological fluids and virulence of desiccated A. baumannii *cells*

Given that the vast majority of *A. baumannii* cells are in the VBNC state after 1-week desiccation (Figure 2b), we wondered if resuscitation also occurs in biological fluids, as this would be a pre-requisite for ensuing *in vivo* proliferation. Since biological fluids contain carbon sources that would sustain bacterial replication during 24-h incubation at 37°C, we tested *A. baumannii* resuscitation in heat-inactivated human serum (HIS), urine, and saliva supplemented with bacteriostatic concentrations of ciprofloxacin (Cip) to prevent bacterial growth (Figure 3a). After desiccation, only ATCC 19606^T was resuscitated in saliva, whereas both ATCC 19606^T and ACICU were resuscitated in HIS and urine (Figure 3b), raising the possibility that desiccated *A. baumannii* cells which contaminate the hospital environment can resuscitate in human biological fluids to cause infection. Consequently, the virulence potential of both *A. baumannii* strains before and after desiccation, and after resuscitation in M9SS $Mg^{2+}Ca^{2+}$ or biological fluids, was tested in the *Galleria mellonella* insect model of infection. Although desiccated cells of both strains were significantly less virulent than the non-desiccated counterparts, virulence was fully recovered after resuscitation in biological fluids (Figure 3c). The reduced virulence of desiccated cells suggests that part of the bacterial inoculum is unable to replicate *in vivo* and/or is cleared by the insect immune system before resuscitation. Overall, these data demonstrate that the VBNC *A. baumannii* population retains infectivity and lethality in the insect model of infection after resuscitation in biological fluids.

Transcriptional reprogramming in desiccated A. baumannii *cells*

To gain insights into the regulatory mechanisms implicated in the transition to the VBNC state, the transcriptional profiles of ATCC 19606^T and ACICU were compared before and after 1-week desiccation by RNA-sequencing (Figure 4a). Desiccation caused an extensive transcriptional reprogramming, involving *ca.* one-third of *A. baumannii* genes (Table S1). ACICU showed more differentially expressed genes (DEGs) than ATCC 19606^T (1,101 *vs* 975, respectively). Of the 539 DEGs shared by the two strains, only 9 showed opposite regulation (Figure 4b). To shed light on the functional categories of shared DEGs, each DEG was assigned to a cluster of orthologous groups of protein (COG) category (Table S2). COGs within the P (inorganic ion transport and metabolism) and C (energy production and conversion) categories were enriched with upregulated DEGs (Figure 4c; Table S3). The downregulated DEGs were enriched in COGs related to the J (translation, including ribosome structure and biogenesis) and O (molecular chaperones and related functions) categories (Figure 4c; Table S4). The Kyoto Encyclopedia of Genes and Genomes (KEGG) pathway analysis indicated that the upregulated DEGs common to both strains were enriched in pathways involving ATP-binding cassette (ABC) transporters (ko02010), sulphur and biotin metabolism (ko00920 and ko00780, respectively), and fatty acid biosynthesis (ko00061) (Figure 4d; Table S5). The shared downregulated DEGs enriched the pathways related to ribosome biogenesis (ko03010), valine, leucine, and isoleucine degradation (ko00280), benzoate degradation (ko00362), and geraniol degradation (ko00281) (Figure 4e; Table S6).

Involvement of L-cysteine, L-glutamate, and glyoxylate shunt pathway in A. baumannii *desiccation resistance and resuscitation*

Analysis of individual DEGs belonging to upregulated COG categories (P and C) and KEGG pathways (ABC transporters and sulphur metabolism) shared by ATCC

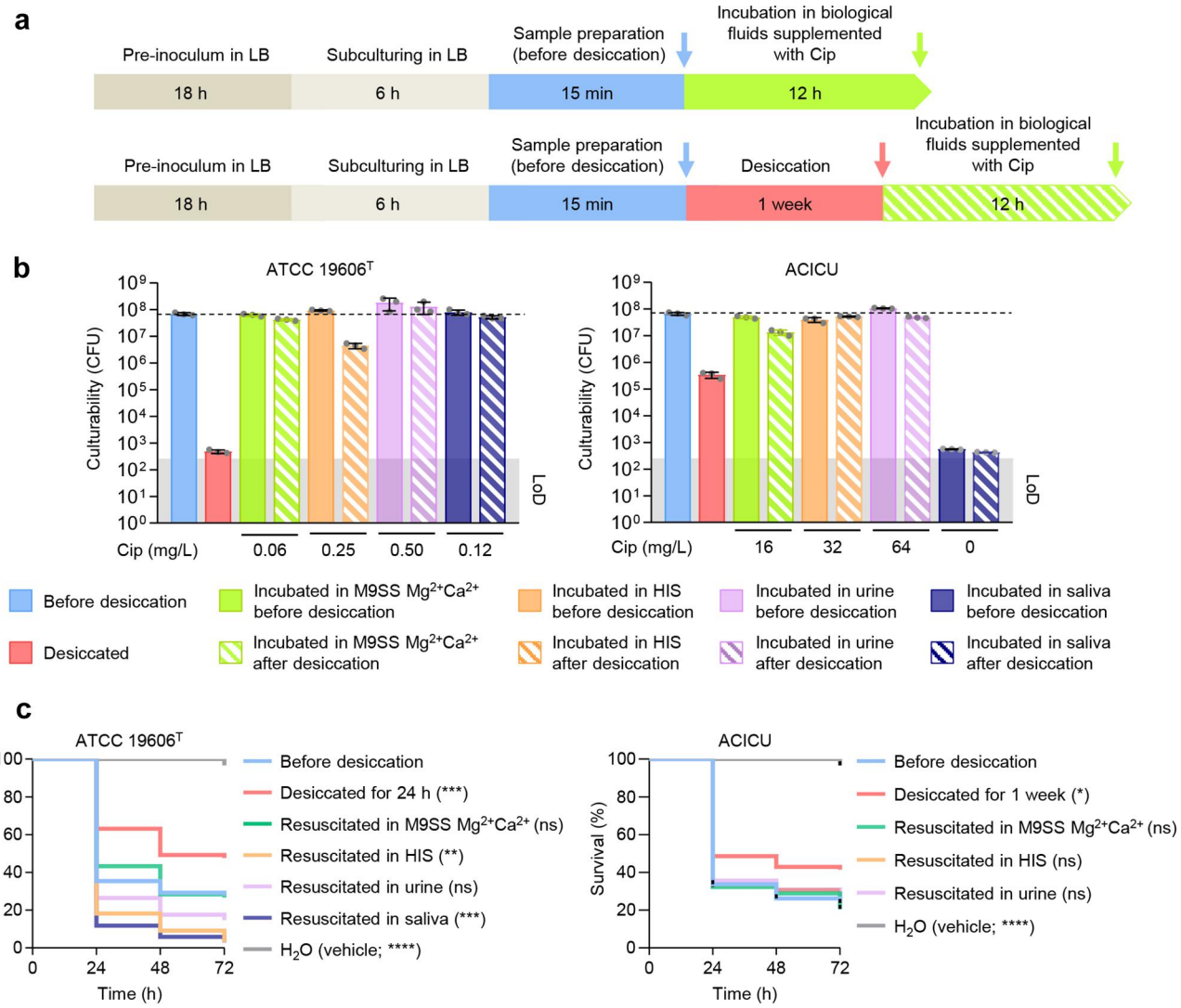

Figure 3. Resuscitation of desiccated *A. baumannii* cells in different biological fluids, and lethality in an insect infection model. (a) Experimental timeline of the resuscitation assay in different biological fluids. Colored arrows indicate the sampling times for CFU counts; cyan, before desiccation; red, after desiccation; fluo-green, after resuscitation. (b) Suspensions of ATCC 19606^T and ACICU cells before and after 1-week desiccation were incubated at 37°C for 12 h in HIS, urine, or saliva supplemented with Cip. The concentrations shown beneath the bars indicate the bacteriostatic concentration of Cip for each resuscitation medium. M9SS $Mg^{2+}Ca^{2+}$ was used as the resuscitation control medium. After incubation, clonogenicity was evaluated by CFU counts. Color codes of histograms are those used in the experimental timeline. The grey area indicates the LoD of CFU counts (4×10^2 CFU). Dashed lines indicate the pre-desiccation values. Data are the mean±SD (error bars) of three independent experiments. (c) Lethality of ATCC 19606^T and ACICU cells in *G. mellonella*. The larvae ($n = 120$ per group) were injected with *A. baumannii* cells taken before desiccation, after desiccation, and after resuscitation in M9SS $Mg^{2+}Ca^{2+}$, HIS, urine, or saliva. Ten µL of bacterial suspensions at $OD_{600} = 0.1$ (*ca.* 5×10^6) and $OD_{600} = 0.01$ (*ca.* 5×10^5) for ATCC 19606^T and ACICU, respectively, corresponding to the LD_{50} of each strain, were inoculated into each caterpillar. After injection, larvae were kept at 37°C, and their survival was monitored every 24 h for 3 days. p-values were determined by the log-rank test (ns, not significant; *$p < 0.05$; **$p < 0.01$; ***$p < 0.001$; ****$p < 0.0001$). Asterisks indicate statistically significant differences between the survival plots of larvae infected with ATCC 19606^T and ACICU cells before desiccation and the test condition.

19606^T and ACICU, unveiled a metabolic flux of sulphur- and carbon-containing compounds towards the biosynthesis of L-cysteine, L-glutamate, and glyoxylate (Figure 5a). The upregulation of genes encoding ABC transporters of sulphur compounds (*cysPUWA*, *tauABC*, and *ssuABC* for sulphate, taurine, and alkanesulfonate uptake, respectively) and enzymes implicated in the conversion of dimethylsulfone to sulphite (*ssuD*, *ssuE*, and *sfnG*) direct the metabolism towards the generation of sulphite, a central precursor of L-cysteine. Furthermore, the upregulation of both *cysJ* and *cysE* would increase the production of sulphide

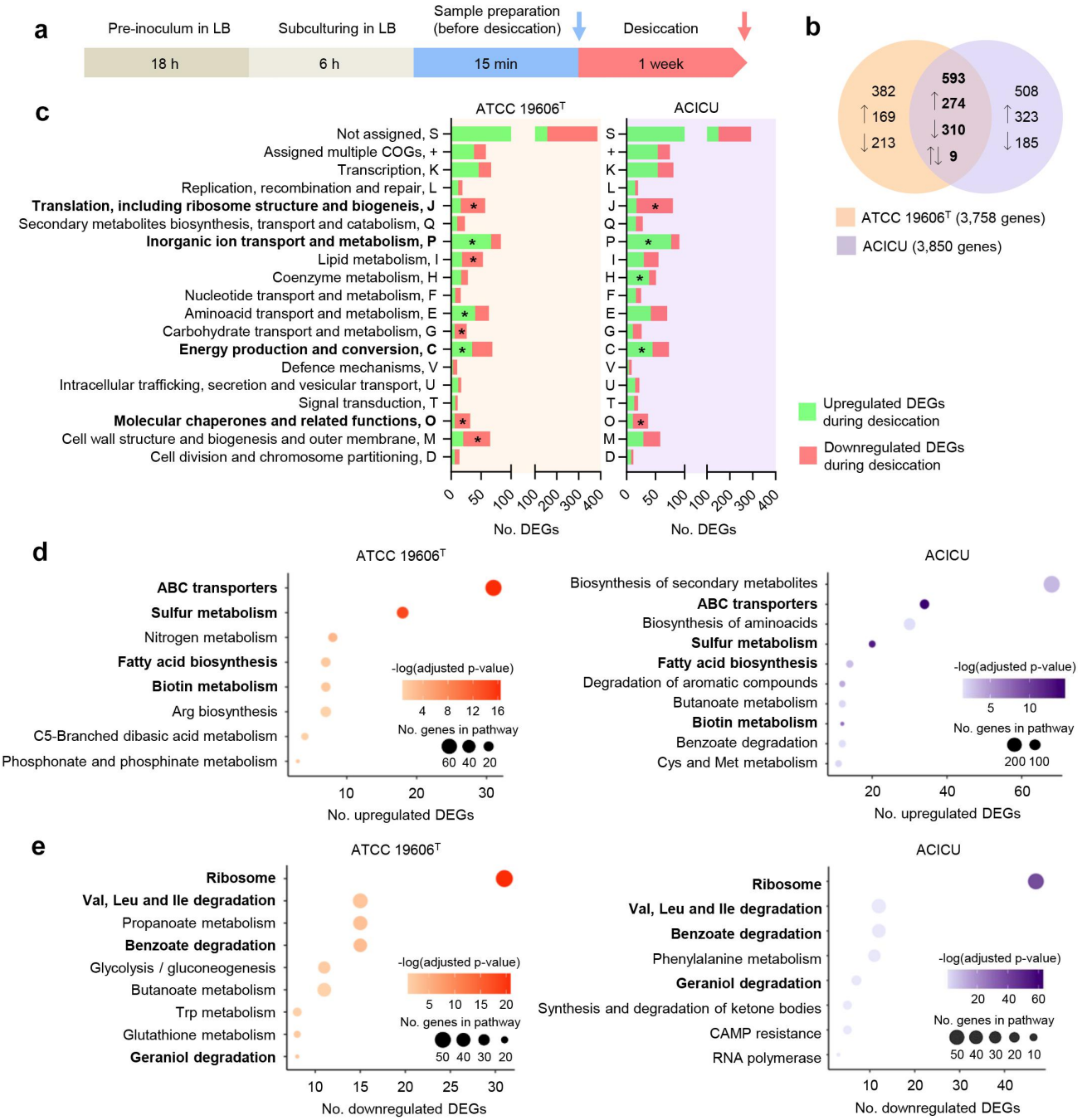

Figure 4. Analysis of the *A. baumannii* transcriptome before and after desiccation. (a) Timeline of sample collection for transcriptome analysis. Arrows indicate the sampling times of cells for RNA-seq before (cyan) and after (red) desiccation. (b) Venn diagram showing the number of DEGs in ATCC 19606^T and ACICU after 1-week desiccation. The number of shared DEGs is shown in bold. Upwards and downwards arrows indicate up- and down-regulated DEGs, respectively. (c) COG functional categories of ATCC 19606^T and ACICU DEGs in desiccated cells. Asterisks in green and red bars denote COGs enriched with up- and down-regulated DEGs, respectively. Shared categories are highlighted in bold. (d-e) KEGG pathway-based enrichment analysis of upregulated (d) and downregulated (e) DEGs of ATCC 19606^T and ACICU during desiccation. Shared pathways are highlighted in bold. Abbreviations: ABC, ATP-binding cassette; CAMP, cationic antimicrobial peptide.

(resulting from sulphite oxidation catalysed by CysJ) and O-acetylserine (generated from L-serine by CysE), respectively, both serving as substrates for the biosynthesis of L-cysteine and acetate (Figure 5a). Upregulation of genes involved in L-cysteine biosynthesis was confirmed by reverse transcription-quantitative PCR (RT-qPCR) analysis of *cysU*, *sfnG*, *ssuE*, *cysJ*, and *cysE* transcripts. All five genes were upregulated in both ATCC

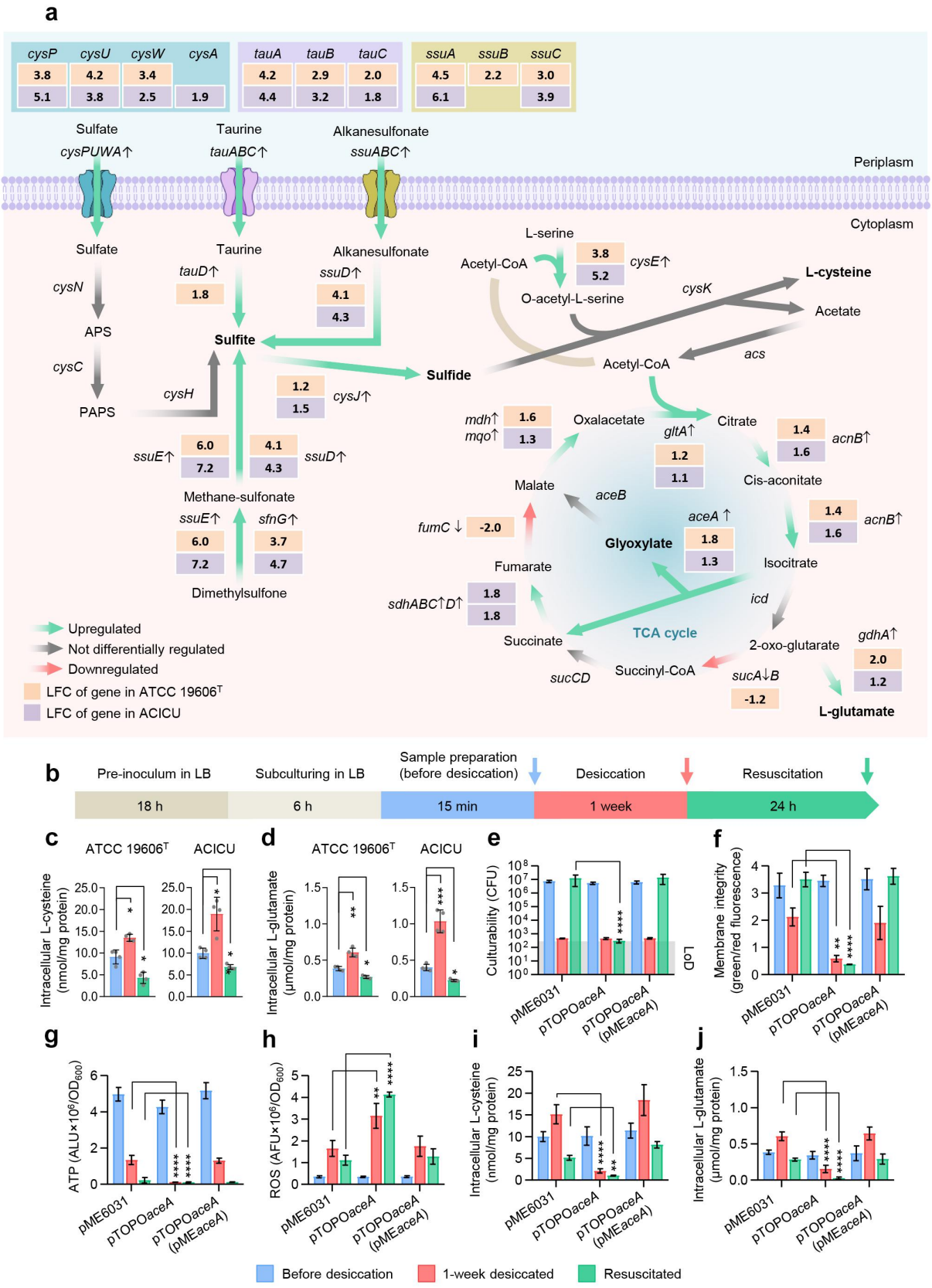

Figure 5. Role of L-cysteine, L-glutamate, and GS pathway in *A. baumannii* desiccation resistance. (a) Schematic representation of the sulfur metabolism, TCA, and GS pathway, with relevant metabolites in bold. Values in orange and purple boxes indicate the $\log_2$ fold-change (LFC) of ATCC 19606^T and ACICU DEGs, respectively. The LFC value of non-DEGs is not shown. Gene, locus tag, and enzyme designations are provided in Figure S10. (b) Experimental timeline. Colored arrows indicate the sampling times for cells

19606^T and ACICU during desiccation, and downregulated or not differentially expressed during resuscitation (Figure S10), paralleling the increase of intracellular L-cysteine levels occurring during desiccation and its consumption during resuscitation (Figure 5b-c). Acetate is converted into acetyl-CoA by acetyl-CoA synthetase (Acs), serving as substrate for CysE or entering the tricarboxylic acid (TCA) cycle. Notably, DEGs involved in the glyoxylate shunt (GS) pathway, namely *gltA* (citrate synthase), *acnB* (aconitase), and *aceA* (isocitrate lyase), were upregulated during desiccation in both strains (Table S7). Moreover, the repression of *sucA* (α-ketoglutarate dehydrogenase) concomitant with the activation of *gdhA* (glutamate dehydrogenase) suggests a metabolic flux towards L-glutamate production from 2-oxo-glutarate (Table S7; Figure 5a). RT-qPCR analysis of *gltA*, *acnB*, *aceA*, and *gdhA* transcripts confirmed the upregulation of glutamate synthesis and GS pathway genes in desiccated cells of both ATCC 19606^T and ACICU and showed that these genes were expressed below the basal level in resuscitated cells (Figure S10). Accordingly, intracellular L-glutamate levels significantly increased during desiccation and decreased during resuscitation in both strains (Figure 5d), while the levels of trehalose and D-mannitol, two compatible solutes that accumulate during salt-induced stress [19], remained unchanged (Figure S11). Overall, gene expression analysis and chemical assays suggest that desiccated *A. baumannii* cells activate the GS pathway and overproduce L-cysteine and L-glutamate, whereas resuscitated cells shut off the GS pathway and consume both amino acids.

To substantiate the importance of the GS pathway in the *A. baumannii* response to desiccation, the *aceA* gene, encoding the key enzyme that deviates the TCA cycle to the GS pathway by converting isocitrate into glyoxylate plus succinate, was inactivated in ATCC 19606^T. Knock-out of *aceA* severely impaired the resuscitation efficiency without affecting post-desiccation culturability (Figure 5e). This result indicates that activation of the GS pathway during desiccation ensures the recovery of the clonogenic ability upon resuscitation. Compared with the wild type, desiccated cells of the *aceA* mutant did not recover from membrane damage appearing extremely permeable to PI even after resuscitation (Figure 5f). The *aceA* knock-out also endured severe ATP, L-cysteine, and L-glutamate depletion, and increased ROS production (Figure 5g-j). Complementation *in trans* of the *aceA* mutation rescued the defect in resuscitation, improved membrane integrity, and restored wild-type levels of ATP, ROS, L-cysteine, and L-glutamate (Figure 5e-j).

Discussion

Microorganisms have the exceptional ability to endure harsh environments and adapt to changes in external conditions. Dehydration, induced by either water evaporation (desiccation or matric stress) or exposure to high solute concentrations (hyperosmotic stress), poses a serious challenge to microorganisms. Although both matric and hyperosmotic stresses result in water subtraction from the cell, these two stresses are mechanistically distinct. While dehydration can be obtained by exposing cells to a hypertonic solution, it should be noted that water is still physically present around the cell during hyperosmotic stress. Conversely, air-desiccated cells are not suspended in a water solution, implying that several vital functions are impaired as the result of water evaporation, particularly nutrient diffusion and solute transport, which are indeed essential for the hyperosmotic stress response [3,20]. These differences require distinct adaptive responses as evidenced by the accumulation of different metabolites: while D-mannitol and trehalose protect *A. baumannii* cells during hyperosmotic stress [19], we identified L-cysteine and L-glutamate as possible protectants during desiccation. Based on these differences, our experimental set-up was intended to mimic the *A. baumannii* response to air-drying that would occur when bacterial cells are shed in the hospital environment. To account,

before desiccation (cyan), after desiccation (red), and after resuscitation in M9SS $Mg^{2+}Ca^{2+}$ for 24 h at 37°C (green). (c) L-cysteine concentration in ATCC 19606^T and ACICU cells. (d) L-glutamate concentration in ATCC 19606^T and ACICU cells. (e) Culturability, (f) membrane integrity, (g) ATP content, (h) ROS levels, (i) intracellular L-cysteine, and (j) L-glutamate concentration in wild type and *aceA*-defective ATCC 19606^T strains before desiccation, after desiccation, and after resuscitation. The grey area in (e) indicates the LoD of CFU counts (4×10^2 CFU). Data in (c-j) are the mean±SD (error bars) of at least three independent experiments. Statistical significance was determined by the unpaired *t*-test (*$p < 0.05$; **$p < 0.01$; ***$p < 0.001$; ****$p < 0.0001$). Asterisks in (c-d) indicate statistically significant differences relative to cells before desiccation. Asterisks in (e-j) indicate statistically significant differences between the test strain and ATCC 19606^T(pME6031).

at least in part, for the intra-species *A. baumannii* variability [3], experiments were conducted using the laboratory-adapted type strain ATCC 19606^T [21] and the epidemic isolate ACICU [22], which belongs to International Clonal Lineage II and represents the most widespread *A. baumannii* lineage [23].

While the drying process is a complex phenomenon impacting all macromolecular components of the cell [18], recent findings have linked the gradual loss of *A. baumannii* culturability occurring during desiccation to membrane gelification, a physical process in which phospholipids of both inner and outer membranes become densely packed, stiffening the membranes and leading to membrane ruptures [24,25]. At the functional level, we observed that desiccation causes progressive loss of membrane integrity with volume reduction, ATP depletion, and oxidative stress, ultimately resulting in a dramatic loss of clonogenicity in both ATCC 19606^T and ACICU strains. While the two *A. baumannii* model strains used in this study showed remarkable differences in the timing of their response to the desiccation, it is worth noting that >90% of the population became unculturable after 24-h desiccation on an inert glass substrate, disclosing structural and functional features suggestive of cell death. However, the whole non-culturable *A. baumannii* population, including apparently dead cells characterized by extensively compromised membrane integrity, was able to recover clonogenicity when suspended in a carbon-free physiological buffer, a typical feature of VBNC cells [12]. Resuscitation was optimal under conditions favouring membrane fluidity and stability, *i.e.* optimal temperature (37°C) and availability of membrane-stabilizing divalent cations (Ca^{2+} and Mg^{2+}). Following desiccation, the reversible transition to the VBNC state was demonstrated for several *A. baumannii* clinical strains, as well as strains belonging to non-*A. baumannii* pathogenic species. One can speculate that resistance to desiccation and entrance in the VBNC state are effective survival strategies for species endowed with broad ecological fitness, allowing members of the *Acinetobacter* genus to face harsh conditions and thrive in diverse environments [1,26].

The consequences of the above findings on the transmissibility of *A. baumannii* infection in hospitals can be inferred by the ability of desiccated VBNC cells to resuscitate in some biological fluids and recover their virulence in the *G. mellonella* insect model of infection. The desiccation-induced transition to the VBNC state observed in pathogenic *Acinetobacter* species imposes a paradigm shift in interpreting environmental surveillance results in healthcare settings. Infection control specialists should know that VBNC *Acinetobacter* cells constitute a reservoir of potentially infectious bacteria that cannot be detected in routine monitoring of hospital surfaces through direct culture-based methods.

Although the VBNC state has previously been associated with *A. baumannii* survival to hyperosmotic stress, the underlying molecular mechanisms have been elucidated only in part [10]. Our results suggest that *A. baumannii* extensively remodels its transcriptome when exposed to air-desiccation for one week, *i.e.* when the population consists of >99% VBNC cells. In this condition, comparative transcriptome analysis showed that *ca.* one-third of *A. baumannii* genes are differentially expressed with remarkable differences between ATCC 19606^T and ACICU, suggesting that *A. baumannii* adopts multiple strategies to face desiccation and enter the VBNC state. In search of common response mechanisms to desiccation, we focused on DEGs shared by the two strains, observing that both ATCC 19606^T and ACICU activate genes for the synthesis of L-cysteine and L-glutamate and shift their energetic metabolism towards the GS pathway. The metabolic overview provided by KEGG and COG analysis also denotes a reduction of protein synthesis (ko03010, ribosome) and expression of molecular chaperones (O category, molecular chaperones and related functions), consistent with prior findings [27,28]. Intriguingly, although DtpA and DtpB molecular chaperones appeared essential for resistance to desiccation in a Lon protease-deficient mutant of *A. baumannii* ATCC 17978 [9], in our experimental conditions *dptA* and *dtpB* were not differentially expressed (Table S1). It is plausible that the expression of these two chaperones occurs at different stages of desiccation, is strain-specific, and/or restricted to the Δ*lon* mutant. Even more intriguing is the observation that the catalase gene *katE*, previously hypothesized to play a role in the detoxification of ROS produced during desiccation [9], was downregulated in ATCC 19606^T and not differentially expressed in ACICU (Table S1), raising the possibility that *A. baumannii* employs alternative strategies to withstand the desiccation-induced oxidative stress. Production of antioxidants, like L-cysteine, is a viable defence strategy from oxidative stress, and we provide evidence that L-cysteine is accumulated during desiccation and is consumed during resuscitation. L-cysteine is known to protect bacteria from ROS through S-thiolation, a reversible post-translational modification that links low molecular weight thiols (*e.g.*, L-cysteine and glutathione) to protein sulfhydryl groups via disulfide bonds, safeguarding thiol-

containing proteins from irreversible oxidative damage [29,30].

Transcriptomic and chemical analyses revealed that *A. baumannii* cells overproduce the osmolyte L-glutamate during desiccation, consistent with the upregulation of the L-glutamate dehydrogenase (*gdhA*) gene. Notably, increased L-glutamate synthesis has previously been documented in VBNC cells of ATCC 19606^T induced by hyperosmolarity (Table S8; ref. [10]) and in nutrient-starved VBNC cells of *Vibrio parahaemolyticus* [31], suggesting that overproduction of L-glutamate is a general stress-response mechanism associated with the transition to a quiescence state. Among the *de novo* synthesized compatible solutes, L-glutamate has a broader function in bacterial stress response than trehalose and mannitol, whose function is limited to osmoprotection. Indeed, induction of L-glutamate synthesis has been associated with acid tolerance, growth under oxygen limitation, resistance to lantibiotics, and protection against oxidative stress [32].

A prominent role of the GS pathway in resuscitation from the VBNC state can be inferred from the expression analysis and mutagenesis of *aceA*. By shortcutting the TCA cycle into the GS pathway, desiccating *A. baumannii* cells would slow down their energetic metabolism, consistent with the established role of the GS pathway in the maintenance of the stress-induced latency and VBNC state in other bacterial pathogens [33–35].

It is interesting to notice that in *A. baumannii* the mutational inactivation of the GS pathway has no effect on clonogenicity after desiccation but impairs the resuscitation of desiccated (VBNC) cells. Wild type and *aceA*-mutant cells show a similar decay in clonogenicity after 1-week desiccation, but only the *aceA*-mutant does not resuscitate from the VBNC state. During desiccation, ATP consumption and ROS production increase in the *aceA* mutant compared with the wild type. Concomitantly, the synthesis of protective metabolites (L-cysteine and L-glutamate) is strongly reduced. These metabolic alterations are likely to impair the ability of the *aceA* mutant to relieve the desiccation stress, as shown by a further increase in ROS production and consumption of residual L-cysteine and L-glutamate levels during resuscitation. In addition, *aceA* mutant cells disclose more severe membrane damage during desiccation and are impaired in membrane repair during the resuscitation step. All these features suggest that, following desiccation, the *aceA* mutant cells are dead or enter a deeper state of dormancy that cannot be reversed under the resuscitation conditions of this study.

Master regulators controlling the expression of *A. baumannii* desiccation- and stress-responsive proteins are promising targets for the development of alternative strategies against *A. baumannii* [36–39]. Since resuscitation from the VBNC state is essential for the virulence of desiccated *A. baumannii* cells, inhibition of AceA would represent a novel approach to impede *A. baumannii* resuscitation, "freezing" the cells in the less virulent VBNC state. Notably, itaconate, a lysosomal inducer produced by macrophages in response to bacterial infection [40] acts as a potent AceA inhibitor [41], showcasing how innate immunity has evolved AceA inhibitory strategies to combat bacterial infection.

Materials and methods

Bacterial strains and culture media

The bacterial strains used in this study are listed in Table S9. The *A. baumannii* type strain ATCC 19606 [21] and the *A. baumannii* strain ACICU, a prototype of the epidemic International Clonal Lineage II [22] were used for comparison. *A. baumannii* ATCC 19606^T and ACICU had formerly been categorized as "desiccation-sensitive" and "desiccation-resistant," respectively [13,14]. Bacteria were routinely grown in Luria Bertani broth (LB; 42) or LB supplemented with 1.5% (w/v) agar (LA) at 37°C. Antibiotics were used at the following concentrations for *Escherichia coli* DH5α and *A. baumannii*, respectively: gentamicin (Gm) 10 mg/L and 100 mg/L; tetracycline (Tc) 12.5 mg/L and 100 mg/L; kanamycin (Km) 25 mg/L and 50 mg/L.

Preparation of competent cells

Competent *E. coli* cells were prepared by the rubidium-calcium chloride method and transformed according to the heat shock protocol [42]. Electrocompetent cells of *A. baumannii* were prepared as previously described [43], and plasmids were introduced in ATCC 19606^T and ACICU by electroporation, as reported in ref [43].

Bacterial growth measurements, culturability, and SYTO 9 and PI staining

ATCC 19606^T and ACICU were grown in LB and incubated at 37°C under shaking for 18 h. Bacterial cultures were sub-cultured (1:100 dilution) in a flask and incubated at 37°C under shaking. Bacterial growth was monitored for up to 24 h, measuring the optical density at 600 nm (OD_{600}) in a BioSpectrometer Basic spectrophotometer (Eppendorf). Aliquots of the cultures were collected after 6, 14, and 24 h for colony-forming units (CFU) counts on LA and LIVE/DEAD staining using the BacLight kit, containing SYTO 9 and PI dyes (Thermo Fisher),

according to the manufacturer's instructions. Fluorescence emissions of SYTO 9- and PI-stained samples were quantified using a Spark 10 M microplate reader (Tecan) at the excitation/emission wavelengths of 480/500 nm and 515/635 nm, respectively. Stained samples were observed by using a Leica SP5 inverted confocal laser-scanning microscope (CLSM) equipped with a 63× oil immersion objective.

Preparation of bacterial inocula and desiccation conditions

ATCC 19606^T and ACICU were grown in LB at 37°C for 18 h, diluted 1:100 in the same medium, and incubated at 37°C under shaking for 6 h. Then, bacteria were harvested by centrifugation (3,000 *g* × 5 min), washed twice, and suspended in ultrapure distilled water at the desired OD_{600}. Aliquots of bacterial suspensions were air-dried under the laminar flow hood at 25.19 ± 1.49°C and stored in a 16 L-vacuum bell containing 50 g of silica gel at an average temperature of 20.88 ± 0.59°C and an average relative humidity (RH) of 13.00 ± 5.58%. Bacterial suspensions were desiccated on the surface of glass coverslips (Corning cover glasses, Sigma-Aldrich), glass Petri dishes, and glass chamber slides (4-well on lumox detachable, Sarstedt).

Bacterial culturability during maintenance in water and after desiccation

ATCC 19606^T and ACICU inocula were diluted in ultrapure distilled water to OD_{600} = 1.0 (corresponding to *ca.* 5×10^8 CFU/mL for both strains). The bacterial suspensions (20 µL, *ca.* 10^7 CFU) were poured onto a glass coverslip and air-dried or maintained in ultrapure distilled water (15 mL) in 50 mL-polystyrene tubes (Falcon) and incubated at 20.88 ± 0.59°C for up to 8 weeks. Culturability of desiccated and water-maintained cells was evaluated by CFU counts on LA plates at 0 h, 6 h, 24 h, 48 h, 72 h, 1 week, 2 weeks, 4 weeks, and 8 weeks. Air-dried samples on glass coverslips were rehydrated in 2 mL of ultrapure distilled water, incubated for 15 min at room temperature, mixed by vortexing for 30 s, and 10-fold serially diluted in sterile saline for CFU counts, as previously described [13,14]. To evaluate bacterial culturability in water, 20-µL samples were appropriately diluted for CFU counts on LA plates.

PI toxicity and time-lapse microscopy assessment of bacterial clonogenicity

ATCC 19606^T(pVRL1*gfp*) and ACICU(pVRL1*gfp*) were suspended in ultrapure distilled water and air-dried. Culturability before and after desiccation was assessed by CFU counts on LA. The OD_{600} of samples before and after desiccation was adjusted to inoculate the same number of clonogenic cells (*ca.* 10^5 CFU/mL) in LB containing serial twofold PI dilutions (ranging from 120 µM to 30 µM). Bacterial growth (OD_{600}) at 37°C was monitored over time using the Spark 10 M (Tecan) microplate reader. The subinhibitory PI concentration (60 µM) was determined by comparison of growth profiles of desiccated and non-desiccated cells treated with increasing PI concentrations (30–120 µM).

Time-lapse fluorescence microscopy experiments were performed with a Leica SP5 CLSM equipped with a 63× oil immersion objective. ATCC 19606^T (pVRL1*gfp*) and ACICU(pVRL1*gfp*) were suspended in water, diluted to OD_{600} = 0.5, and air-dried on glass coverslips for 0 h, 6 h, and 24 h. Desiccated bacteria were covered with a 0.1 mm thick layer of LB supplemented with 0.5% (w/v) agarose and 60 µM propidium iodide (PI), and placed in a CLSM incubation chamber at 37°C, 80% RH, and 20% $P(O_2)$. Twenty µL of samples before air-drying were directly deposited on LB 0.5% (w/v) agarose supplemented with 60 µM PI and placed in the CLSM incubation chamber under the same conditions. Time-lapse microscopy images of at least 20 different fields of view (400 µm × 400 µm) were acquired every 30 min for 4 h, since thereafter cells stopped dividing, probably due to lack of nutrients and/or phototoxicity. Due to the low probability of spotting clonogenic cells after long-term desiccation (see Results), 24 h was designated as the desiccation endpoint for clonogenicity assessment.

Automatic cell- and microcolony-counting was performed using CellProfiler [44]. Cells organized in clusters before incubation were manually identified and excluded from the analysis.

Quantification of GFP release during desiccation

ATCC 19606^T(pVRL1*gfp*) and ACICU(pVRL1*gfp*) were suspended in ultrapure distilled water and air-dried on glass Petri dishes for 6 h and 24 h. Cells before and after desiccation were diluted to OD_{600} = 0.5 in ultrapure distilled water and centrifuged (3,000 *g* × 5 min). Supernatants were collected to determine the emission spectra ranging from 500 to 530 nm with a resolution of 0.5 nm employing the LS-50B fluorimeter (PerkinElmer).

Membrane integrity assessment and resuscitation of desiccated cells in different media

Bacterial cells were diluted in ultrapure distilled water up to OD_{600} = 1.0. Twenty µL of the bacterial suspensions were poured onto a glass coverslip and air-dried

for 0 h, 24 h, and 1 week. After desiccation, CFU counts were performed. Alternatively, air-dried bacteria were incubated at 37°C or 4°C for 24 h under shaking in 2 mL of the following resuscitation media: *i*) PBS without calcium chloride and magnesium chloride (Sigma-Aldrich); *ii*) M9 basal salt solution (M9SS) without carbon source (7 g/L Na_2HPO_4, 3 g/L KH_2PO_4, 0.5 g/L NaCl, 1 g/L NH_4Cl; 42); *iii*) PBS supplemented with 1 mM $MgSO_4$ and 0.2 mM $CaCl_2$ (PBS $Mg^{2+}Ca^{2+}$); *iv*) M9SS supplemented with 1 mM $MgSO_4$ and 0.2 mM $CaCl_2$ (M9SS $Mg^{2+}Ca^{2+}$; ref. [42]). After resuscitation, bacterial culturability was evaluated by CFU counts, and bacterial membrane integrity was assessed by SYTO 9/PI staining by using the LIVE/DEAD BacLight kit (Thermo Fisher). Similarly, bacterial culturability and membrane integrity were evaluated during resuscitation, harvesting cells after 6-, 12-, 24-, and 48-h incubation in M9SS $Mg^{2+}Ca^{2+}$ at 37°C.

Membrane integrity was also assessed by the Van susceptibility test. Briefly, ATCC 19606^T and ACICU were washed twice, suspended in ultrapure distilled water, and air-dried on glass Petri dishes for 24 h. An aliquot of desiccated cells was resuscitated for 24 h at 37°C in M9SS $Mg^{2+}Ca^{2+}$. Bacterial samples were resuspended at $OD_{600} = 0.001$ (corresponding to ca. 5×10^5 CFU/mL) in 100 µL of cation-adjusted Mueller Hinton broth (CAMHB; Becton Dickinson) supplemented with increasing concentrations of vancomycin (Van; 512–0.5 mg/L). MIC was defined as the lowest concentration that completely inhibited bacterial growth as detected by the unaided eye, according to Clinical Laboratory Standards Institute recommendations (CLSI, 2024). For Van time-killing assay, bacterial samples were resuspended at $OD_{600} = 0.1$ in saline and saline supplemented with 512 mg/L Van, incubated at 37°C, and plated on LA after 0, 3, 6, 9, and 12 h for CFU counts. For each time, the survival percentages were calculated by dividing the CFU obtained from the Van-treated sample by the CFU obtained from saline.

Plasmid stability

Bacterial cells before, after 1-week desiccation on glass Petri dishes, and after resuscitation at 37°C for 24 h in M9SS $Mg^{2+}Ca^{2+}$ were washed in distilled water and diluted at $OD_{600} = 1$. CFU were determined on LA (N_0) and LA supplemented with the appropriate antibiotic (N_{Ant}). The plasmid stability percentage was expressed as $(N_{Ant}/N_0) \times 100$, as previously reported [43,45].

AFM analysis of bacterial cells and image processing

ATCC 19606^T and ACICU were diluted in ultrapure distilled water to $OD_{600} = 0.5$. Twenty µL of bacterial suspensions were poured onto a microscope glass (Thermo Scientific SuperFrost Microscope slides 76 × 26 mm with 1 mm thickness) and imaged by AFM before and after desiccation, and after resuscitation. AFM measurements were carried out at 24°C using a Dimension ICON AFM (Bruker, Santa Barbara, USA) operating in the PeakForce mode, as previously described with minor modifications [46]. Briefly, the AFM cantilever (Bruker Scan-Asyst-Air) was set for "soft" nominal spring constant of 0.4 N/m and had a sharpened silicon tip with a nominal radius of 2 nm. The cantilever oscillation frequency and oscillation amplitude were set to 1 kHz and 150 nm, respectively. The force set point was optimized in the 15–25 nN range. The image size was 512 pixels/line/row, and the minimum lateral resolution was determined by the scan size. AFM images were analysed with Gwyddion Software v.248 [47]. All images were first-order flattened and set to the same range of height (0–900 nm) to facilitate comparison between conditions. After levelling, a metrological analysis was performed on at least 30 different randomly selected cells to measure their biophysical parameters. Briefly, cellular length and width were referred to as elongated and short horizontal axes, respectively. Cell height was determined based on the maximum height measured along the cell cross-section. Cell volume and surface area were obtained by the Gwyddion grain-analysis algorithm after individual cell masking.

Evaluation of ATP levels and ROS production in cells before desiccation, after desiccation, and after resuscitation

Bacterial cells were washed twice, suspended in ultrapure distilled water, and air-dried for 1 week. After desiccation, the samples were diluted and resuscitated in M9SS $Mg^{2+}Ca^{2+}$. The cellular ATP content was quantified by the BacTiter-Glo Microbial Cell Viability Assay (Promega) according to the manufacturer's instructions. Briefly, the cells taken before and after desiccation or after resuscitation were suspended in 50 µL of ultrapure distilled water, mixed with an equal volume of the BacTiter-Glo reagent, and incubated in the dark for 5 min. Then, luminescence was measured employing the Spark 10 M (Tecan)

microplate reader. The ATP content was expressed as the ratio between arbitrary luminescence units (ALU) and the OD_{600} of the bacterial suspension. ROS levels were quantified by employing the 2,7-dichlorofluorescein diacetate (DCFDA)-based assay [48]. Cells taken before and after desiccation or after resuscitation were suspended in 100 µL of ultrapure distilled water containing 10 µM DCFDA. The fluorescence excitation/emission at 485/535 nm of DCFHDA and the OD_{600} of samples were measured in a Spark 10 M (Tecan) microplate reader. ROS production was expressed as the ratio between arbitrary fluorescence unit (AFU) emission and OD_{600}.

Resuscitation in biological fluids

The biological fluids used in this study are residual samples from previous works [49,50]. An existing stock of heat-inactivated human serum (HIS) pooled from 125 healthy donors was used [49]. Urine and saliva specimens were previously collected from 10 healthy donors, pooled, and filter-sterilized [50]. ATCC 19606^T and ACICU cells were air-dried for 1 week on glass Petri dishes. Cells before and after desiccation were diluted at $OD_{600} = 0.1$ in HIS, urine, saliva, or M9SS $Mg^{2+}Ca^{2+}$ supplemented with different two-fold serially diluted ciprofloxacin (Cip) concentrations ranging from 128 to 0.03 µg/mL. CFU counts were performed after 12-h incubation at 37°C with shaking.

Galleria mellonella *infection assay*

The LD_{50} of ATCC 19606^T and ACICU, corresponding to *ca.* 5×10^6 and 5×10^5 CFU, respectively, was preliminarily determined [51]. Since ATCC 19606^T is more susceptible to desiccation than ACICU (see Results), to appreciate any difference between different resuscitation conditions, the *G. mellonella* killing assay was set up to inject the larvae with bacterial inocula causing *ca.* 50% lethality. To this purpose, ATCC 19606^T and ACICU were washed twice with ultrapure distilled water, air-dried for 24 h and 1 week, respectively, and then incubated in M9SS $Mg^{2+}Ca^{2+}$, HIS, urine, or saliva for 12 h at 37°C. After 24-h and 1-week desiccation, ATCC 19606^T and ACICU showed comparable levels of culturability (see Results). Fifth-instar *G. mellonella* larvae (0.406 ± 0.054 g) were injected with 10 µL of bacterial suspensions before air-drying, after desiccation, or after incubation in M9SS $Mg^{2+}Ca^{2+}$ or biological fluids at $OD_{600} = 0.1$ (*ca.* 5×10^6 CFU) and 0.01 (*ca.* 5×10^5 CFU) for ATCC 19606^T and ACICU, respectively, corresponding to the LD_{50} of the two strains. The *G. mellonella* infection assay was performed as previously described [52], using sterile water as vehicle and control. A cohort of 120 larvae was injected for each experimental group. Larvae unresponsive to multiple tactile stimulations were considered dead.

Isolation and purification of bacterial RNA

ATCC 19606^T and ACICU cells were washed in ultrapure distilled water, suspended in ultrapure distilled water at $OD_{600} = 1.0$, and 4 mL of suspension were uniformly spread on the surface of 78.5 cm^2 glass Petri dishes for one-week desiccation. Before and after desiccation, bacteria were directly suspended in 2 mL of RNA Protect Bacteria Reagent (Qiagen). Total RNA isolation was performed by using miRNeasy Mini Kit (Qiagen), according to the manufacturer's instructions. RNA was purified with RNeasy MiniElute Cleanup Kit (Qiagen), and RNA samples were treated with TURBO DNase (Invitrogen) to remove genomic DNA. PCR reactions were performed to confirm the absence of DNA contamination by using the oligonucleotides 16S_FW and 16S_RV (Table S10). RNA concentration and purity were measured with a NanoDropTM spectrophotometer (Thermo Fisher Scientific). Three independent RNA isolation and purification experiments were performed for each condition.

Genome-wide expression analyses and functional annotations

The RNA-seq analysis, RNA quality assessment, library preparation, sequencing, and statistical analysis of the data were performed at the GENEWIZ Biotechnology Facility (GENEWIZ, Azenta Life Sciences Company, Leipzig, Germany), as previously described [53]. In particular, RNA samples were quantified using the Qubit 4.0 Fluorometer (Life Technologies), and RNA integrity was checked with an RNA kit on an Agilent 5300 Fragment Analyzer (Agilent Technologies). The average RNA integrity numbers ± SD, calculated on three biological replicates for each sample, were as follows: 9.15 ± 0.23, ATCC 19606^T cells before desiccation; 9.13 ± 0.41, ATCC 19606^T cells after 1-week desiccation; 8.95 ± 0.12, ACICU cells before desiccation; 9.01 ± 0.21, ACICU cells after 1-week desiccation. rRNA depletion was performed using the NEB Next rRNA Depletion kit (New England Biolabs). RNA sequencing library preparation was performed using the NEB Next Ultra II RNA Library Prep kit for Illumina, following the manufacturer's recommendations. The library

preparation was not directional. Briefly, enriched RNAs were fragmented according to the manufacturer's instructions. First-strand and second-strand cDNA were subsequently synthesized. cDNA fragments were end-repaired and adenylated at the 3' ends, and a universal adapter was ligated to cDNA fragments, followed by index addition and library enrichment with limited-cycle PCR. Sequencing libraries were validated using the NGS kit on the Agilent 5300 Fragment Analyzer (Agilent Technologies) and quantified using the Qubit 4.0 Fluorometer. The sequencing libraries were multiplexed and loaded onto the flow cell on the Illumina NovaSeq 6000 instrument, according to the manufacturer's instructions. The samples were sequenced using a 2×150 Pair-End configuration v1.5. Image analysis and base calling were conducted by NovaSeq Control Software v1.7 on the NovaSeq instrument. Raw sequence data (.bcl files) generated from Illumina NovaSeq were converted into fastq files and demultiplexed using the Illumina bcl2fastq program v2.20. One mismatch was allowed for index sequence identification. After investigating the quality of the raw data, sequence reads were trimmed to remove possible adapter sequences and nucleotides with poor quality using Trimmomatic v0.36. The trimmed reads were mapped to the reference genome using the Bowtie2 aligner v2.2.6. BAM files were generated as a result of this step. Unique gene hit counts were calculated using feature counts from the Subread package v1.5.2. Only unique reads that fell within gene regions were counted. After gene hit counts extraction, the gene hit counts table was used for downstream differential expression analysis. Using DESeq2, a comparison of gene expression between the customer-defined groups of samples was performed. All RNA-seq reads were aligned to the genome of ATCC 19606^T (NZ_CP058289.1) and ACICU (NZ_CP031380.1) for data analysis. The Wald test was used to generate p-values and $\log_2$ fold-change (LFC). Only genes with an adjusted p-value (p adj)<0.05 were considered differentially expressed genes (DEGs). Plasmid genes were excluded for the comparative gene expression analysis between ATCC 19606^T and ACICU.

The EggNOG-mapper v5.0 [54] was used to determine the COG categories [55] and Kyoto Encyclopaedia of Genes and Genomes (KEGG) pathways [56]. All selected DEGs were visualized within their relative metabolic pathway using the KEGG Mapper-Reconstruct tool, in the KEGG pathway database [56]. Enrichment analysis of DEGs in COG categories and KEGG pathways was performed with the "enrichr" function from the clusterProfiler package v4.0 [57]. Annotations of EggNOG-mapper v5.0 (.emapper.annotations) were used to develop the corresponding reference databases. *p*-values were adjusted for multiple comparisons using the false discovery rate algorithm. The bubble plots illustrating significantly enriched pathways (*p*-value <0.05) were drawn with the R package ggplot2.

Reverse-transcriptase quantitative PCR analysis

To determine RNA expression levels of the *cysU*, *sfnG*, *ssuE*, *cysJ*, *cysE*, *gltA*, *acnB*, *aceA*, and *gdhA* genes, cDNA synthesis was performed using the iScript Reverse Transcription Supermix Kit (Bio-Rad). RT-qPCR reactions were performed using the iTaq Universal SYBR Green Supermix (Bio-Rad). Gene-specific primers used for the analysis are listed in Table S10. The 16S rRNA gene was used as an internal control to normalize the RT-qPCR data and to calculate the relative fold change in gene expression by using the $2^{-\Delta\Delta CT}$ method, as previously described [52]. RT-qPCR analysis was performed on three different RNA pools for each condition (biological replicates).

Disruption of the aceA gene and genetic complementation of the aceA mutation

A 517-bp DNA fragment internal to the ATCC 19606^T *aceA* gene (HTZ92_RS12445) was generated by PCR with aceATOPO_FW and aceATOPO_RV primers (Table S10) for direct cloning in pCR-BluntII-TOPO [58], yielding pTOPO*aceA* (Table S9). pTOPO*aceA* was used as an integrative suicide vector in ATCC 19606^T, and the *aceA* knock-out mutants were selected on LA plates containing Km. Disruption of *aceA* was verified by PCR using the M13_FW and aceATOPO_RV primers (Table S10) and amplicon sequencing. The *aceA* knock-out mutant, designated ATCC 19606^T pTOPO*aceA*, was grown in the presence of Km to stabilize the *aceA* mutation [58]. To complement the *aceA* mutation, the entire *aceA* gene with its endogenous promoter was amplified from ATCC 19606^T genomic DNA with primers listed in Table S10. The 2107-bp amplicon was digested using BamHI and EcoRI and cloned into the BglII and EcoRI sites of pME6031 [59], yielding the pME*aceA* plasmid (Table S9). pME*aceA* was introduced in ATCC 19606^T(pTOPO*aceA*) by electrotransformation.

Quantification of compatible solutes and L-cysteine

Bacterial cells before, after 1-week desiccation on glass Petri dishes, and after resuscitation at 37°C for 24 h in M9SS $Mg^{2+}Ca^{2+}$ were diluted at $OD_{600} = 2.0$ in 1 mL of distilled water. Bacterial suspensions were centrifuged (3,000 *g* × 5 min), and pellets were stored at −80°C until used. An aliquot of the bacterial pellet was used to quantify the total protein content with the Coomassie protein assay reagent (Sigma Aldrich) [52]. Another aliquot was frozen at −80°C and thawed at room temperature three times to facilitate cell lysis. For quantification of compatible solutes, the intracellular concentrations of L-glutamate, trehalose, and D-mannitol were determined using L-Glutamic Acid Assay Kit (Megazyme, Neogene), Trehalose Assay Kit (Megazyme, Neogene), and D-Mannitol Assay Kit (Megazyme, Neogene), respectively, following the manufacturer's instructions. Intracellular L-cysteine was quantified using Cysteine Assay Kit (Fluorometric) (Sigma-Aldrich), according to the manufacturer's instructions. The levels of L-glutamate, trehalose, D-mannitol, and L-cysteine were normalized to the total protein content of each sample.

Statistical analysis

Statistical analysis was performed with the GraphPad Instat software v8.0. Survival curves were generated by the Kaplan–Meier method, and the significance of survival differences was estimated by the log rank test. Differences having a *p*-value ≤0.05 were considered statistically significant. All *in vitro* experiments were analysed using a two-tailed unpaired student's *t*-test.

Ethical statement

The use of human-derived samples was conducted according to the Helsinki Declaration statement of ethical principles. In particular, the biological fluids used in this study are by-products from previous works, upon approval by the review board of Policlinico Umberto I, Sapienza University, Rome [49,50]. Human serum, urine, and saliva samples were obtained from healthy donors, following illustration, approval, and subscription of informed consent. Then, samples were anonymously submitted to the laboratory, pooled, and used for experimental purposes.

Acknowledgements

A preliminary version of this manuscript has been published as a pre-print on SSRN (doi: 10.2139/ssrn.4731192; licenced under CC BY 4.0). Data from this paper were also presented as a conference talk with interim findings at the "13th Symposium on the Biology of Acinetobacter," and the corresponding abstract was published at https://13acinetobacter.organideia.pt/wp/book-of-abstracts-2/.

Disclosure statement

No potential conflict of interest was reported by the author(s).

Funding

This work was partly supported by the Excellence Department grant [art. 1, comma 314–337 Legge 232/2016] to the Department of Science, Roma Tre University from Ministero dell'Università e della Ricerca and by grant A0375-2020-36558 GAVAP from Regione Lazio to PV. PV also acknowledges the financial support of Rome Technopole [grant F83B22000040006] for transcriptomic analyses. ML was supported by a NBFC fellowship [grant CN00000033] funded by Ministero dell'Università e della Ricerca. The funders had no role in study design, data collection, interpretation, or the decision to submit the work for publication.

CRediT authorship contribution statement

Lucidi Massimiliano: Conceptualization, Data curation, Investigation, Methodology, Validation, Visualization, Writing – original draft, Writing – review and editing.

Capecchi Giulia: Data curation, Investigation, Methodology, Writing – original draft.

Spagnoli Cinzia: Data curation, Investigation, Methodology.

Basile Arianna: Data curation, Investigation.

Artuso Irene: Data curation, Investigation.

Persichetti Luca: Data curation, Investigation.

Fardelli Elisa: Data curation, Investigation.

Capellini Giovanni: Supervision, Validation, Writing – review and editing.

Visaggio Daniela: Conceptualization, Project administration, Supervision, Writing – original draft.

Imperi Francesco: Conceptualization, Validation, Writing – review and editing.

Rampioni Giordano: Conceptualization, Validation, Writing – review and editing.

Leoni Livia: Conceptualization, Validation, Writing – review and editing.

Visca Paolo: Conceptualization, Funding acquisition, Investigation, Methodology, Project administration, Validation, Writing – review and editing.

Lucidi Massimiliano and Capecchi Giulia contributed equally to this study as co-first authors.

All authors have read and approved the manuscript.

Data availability statement

Raw data that support the findings of this study, the Supplementary Tables S1-S10, and the Supplementary Video S1 and S2 are openly available in the Open Science Framework (OSF) repository at https://osf.io/g9rf4/ (DOI: 10.17605/OSF.IO/G9RF4). Transcriptomic data have been deposited in the Gene Expression Omnibus database under the accession number GSE249021.

ORCID

Massimiliano Lucidi http://orcid.org/0000-0003-3238-9164
Giulia Capecchi http://orcid.org/0000-0002-0304-6712
Luca Persichetti http://orcid.org/0000-0001-6578-254X
Elisa Fardelli http://orcid.org/0000-0002-4181-1841
Giovanni Capellini http://orcid.org/0000-0002-5169-2823
Daniela Visaggio http://orcid.org/0000-0002-3192-8974
Giordano Rampioni http://orcid.org/0000-0002-1735-8565
Livia Leoni http://orcid.org/0000-0002-2046-4297
Paolo Visca http://orcid.org/0000-0002-6128-7039

References

[1] Dijkshoorn L, Nemec A, Seifert H. An increasing threat in hospitals: multidrug-resistant *Acinetobacter baumannii*. Nat Rev Microbiol. 2007;5(12):939–951. doi: 10.1038/nrmicro1789

[2] Tacconelli E, Carrara E, Savoldi A, et al. Discovery, research, and development of new antibiotics: the WHO priority list of antibiotic-resistant bacteria and tuberculosis. Lancet Infect Dis. 2018;18:318–327. doi: 10.1016/S1473-3099(17)30753-3

[3] Lucidi M, Visaggio D, Migliaccio A, et al. Pathogenicity and virulence of *Acinetobacter baumannii*: factors contributing to the fitness in healthcare settings and the infected host. Virulence. 2024;15(1):2289769. doi: 10.1080/21505594.2023.2289769

[4] Zhang H, Zhang Y, Wu J, et al. Risks and features of secondary infections in severe and critical ill COVID-19 patients. Emerg Microbes Infect. 2020;9(1):1958–1964. doi: 10.1080/22221751.2020.1812437

[5] Ellis RC, Roberts EK, Grier JT, et al. *Acinetobacter baumannii* infections that are resistant to treatment: warning signs from the COVID-19 pandemic. Future Microbiol. 2022;17(17):1345–1347. doi: 10.2217/fmb-2022-0153

[6] van den Broek PJ, Arends J, Bernards AT, et al. Epidemiology of multiple *Acinetobacter* outbreaks in the Netherlands during the period 1999–2001. Clin Microbiol Infect. 2006;12:837–843. doi: 10.1111/j.1469-0691.2006.01510.x

[7] Doughty EL, Liu H, Moran RA, et al. Endemicity and diversification of carbapenem-resistant *Acinetobacter baumannii* in an intensive care unit. Lancet Reg Health West Pac. 2023;37:100780. doi: 10.1016/j.lanwpc.2023.100780

[8] Zeidler S, Müller V. Coping with low water activities and osmotic stress in *Acinetobacter baumannii*: significance, current status and perspectives. Environ Microbiol. 2019;21(7):2212–2230. doi: 10.1111/1462-2920.14565

[9] Green ER, Fakhoury JN, Monteith AJ, et al. Bacterial hydrophilins promote pathogen desiccation tolerance. Cell Host Microbe. 2022;30(7):975–987.e7. doi: 10.1016/j.chom.2022.03.019

[10] König P, Wilhelm A, Schaudinn C, et al. The VBNC state: a fundamental survival strategy of *Acinetobacter baumannii*. MBio. 2023;14:e0213923. doi: 10.1128/mbio.02139-23

[11] Rawlinson S, Ciric L, Cloutman-Green E. How to carry out microbiological sampling of healthcare environment surfaces? A review of current evidence. J Hosp Infect. 2019;103:363–374. doi: 10.1016/j.jhin.2019.07.015

[12] Liu J, Yang L, Kjellerup BV, et al. Viable but nonculturable (VBNC) state, an underestimated and controversial microbial survival strategy. Trends Microbiol. 2023;31(10):1013–1023. doi: 10.1016/j.tim.2023.04.009

[13] Jawad A, Seifert H, Snelling AM, et al. Survival of *Acinetobacter baumannii* on dry surfaces: comparison of outbreak and sporadic isolates. J Clin Microbiol. 1998;36(7):1938–1941. doi: 10.1128/JCM.36.7.1938-1941.1998

[14] Giannouli M, Antunes LCS, Marchetti V, et al. Virulence-related traits of epidemic *Acinetobacter baumannii* strains belonging to the international clonal lineages I-III and to the emerging genotypes ST25 and ST78. BMC Infect Dis. 2013;13(1):282. doi: 10.1186/1471-2334-13-282

[15] Sabatini A, Lucidi M, Ciolfi S, et al. Innate immune mechanisms promote human response to *Acinetobacter baumannii* infection. Eur J Immunol. 2024;54(11):e2451170. doi: 10.1002/eji.202451170

[16] Yang F, Moss LG, Phillips GN. The molecular structure of green fluorescent protein. Nat Biotechnol. 1996;14(10):1246–1251. doi: 10.1038/nbt1096-1246

[17] Geisinger E, Mortman NJ, Dai Y, et al. Antibiotic susceptibility signatures identify potential antimicrobial targets in the *Acinetobacter baumannii* cell envelope. Nat Commun. 2020;11(1):4522. doi: 10.1038/s41467-020-18301-2

[18] Lebre PH, De Maayer P, Cowan DA. Xerotolerant bacteria: surviving through a dry spell. Nat Rev Microbiol. 2017;15:285–296. doi: 10.1038/nrmicro.2017.16

[19] Zeidler S, Müller V. Unusual deprivation of compatible solutes in *Acinetobacter baumannii*. Environ Microbiol. 2020;22:1370–1380. doi: 10.1111/1462-2920.14951

[20] Bosch J, Varliero G, Hallsworth JE, et al. Microbial anhydrobiosis. Environ Microbiol. 2021;23(11):6377–6390. doi: 10.1111/1462-2920.15699

[21] Artuso I, Lucidi M, Visaggio D, et al. Genome diversity of domesticated *Acinetobacter baumannii* ATCC 19606^{T} strains. Microb Genom. 2022;8. doi: 10.1099/mgen.0.000749

[22] Iacono M, Villa L, Fortini D, et al. Whole-genome pyrosequencing of an epidemic multidrug-resistant *Acinetobacter baumannii* strain belonging to the European clone II group. Antimicrob Agents Chemother. 2008;52(7):2616–2625. doi: 10.1128/AAC.01643-07

[23] Roberts LW, Hoi LT, Khokhar FA, et al. Genomic characterisation of multidrug-resistant *Escherichia coli*. *Klebsiella pneumoniae*, and *Acinetobacter baumannii* in two intensive care units in Hanoi, Vietnam: a prospective observational cohort study. Lancet Microbe. 2022;3:e857–66. doi: 10.1016/S2666-5247(22)00181-1

[24] Fardelli E, Lucidi M, Di Gioacchino M, et al. Biophysical mechanisms of dehydrating membranes of *Acinetobacter baumannii* linked to drought-resistance. Biochim et Biophys Acta (BBA) - Biomembr. 2022;1864(12):184045. doi: 10.1016/j.bbamem.2022.184045

[25] Fardelli E, Di Gioacchino M, Lucidi M, et al. Evidence of correlation between membrane phase transition and clonogenicity in dehydrating *Acinetobacter baumannii*: a combined micro-raman and AFM study. J Phys Chem B. 2024;128(28):6806–6815. doi: 10.1021/acs.jpcb.4c01246

[26] Pulami D, Kämpfer P, Glaeser SP. High diversity of the emerging pathogen *Acinetobacter baumannii* and other *Acinetobacter* spp. In raw manure, biogas plants digestates, and rural and urban wastewater treatment plants with system specific antimicrobial resistance profiles. Sci Total Environ. 2023;859:160182. doi: 10.1016/j.scitotenv.2022.160182

[27] Gayoso CM, Mateos J, Méndez JA, et al. Molecular mechanisms involved in the response to desiccation stress and persistence in *Acinetobacter baumannii*. J Proteome Res. 2014;13:460–476. doi: 10.1021/pr400603f

[28] Wang X, Cole CG, Cd D, et al. Protein aggregation is associated with *Acinetobacter baumannii* desiccation tolerance. Microorganisms. 2020;8:343. doi: 10.3390/microorganisms8030343

[29] Ansong C, Wu S, Meng D, et al. Top-down proteomics reveals a unique protein S-thiolation switch in *Salmonella* Typhimurium in response to infection-like conditions. Proc Natl Acad Sci USA. 2013;110:10153–10158. doi: 10.1073/pnas.1221210110

[30] Loi VV, Rossius M, Antelmann H. Redox regulation by reversible protein S-thiolation in bacteria. Front Microbiol. 2015;6:187. doi: 10.3389/fmicb.2015.00187

[31] Wagley S, Morcrette H, Kovacs-Simon A, et al. Bacterial dormancy: a subpopulation of viable but non-culturable cells demonstrates better fitness for revival. PloS Pathog. 2021;17(1):e1009194. doi: 10.1371/journal.ppat.1009194

[32] Feehily C, Karatzas KAG. Role of glutamate metabolism in bacterial responses towards acid and other stresses. J Appl Microbiol. 2013;114(1):11–24. doi: 10.1111/j.1365-2672.2012.05434.x

[33] Nandakumar M, Nathan C, Rhee KY. Isocitrate lyase mediates broad antibiotic tolerance in *Mycobacterium tuberculosis*. Nat Commun. 2014;5:4306. doi: 10.1038/ncomms5306

[34] Bhusal RP, Barr JJ, Subedi D. A metabolic perspective into antimicrobial tolerance and resistance. Lancet Microbe. 2022;3:e160–1. doi: 10.1016/S2666-5247(22)00006-4

[35] Qi Z, Sun N, Liu C. Glyoxylate cycle maintains the metabolic homeostasis of *Pseudomonas aeruginosa* in viable but nonculturable state induced by chlorine stress. Microbiol Res. 2023;270:127341. doi: 10.1016/j.micres.2023.127341

[36] Farrow JM, Wells G, Pesci EC. Desiccation tolerance in *Acinetobacter baumannii* is mediated by the two-component response regulator BfmR. PLOS ONE. 2018;13:e0205638. doi: 10.1371/journal.pone.0205638

[37] Perez Mora B, Giordano R, Permingeat V, et al. BfmRS encodes a regulatory system involved in light signal transduction modulating motility and desiccation tolerance in the human pathogen *Acinetobacter baumannii*. Sci Rep. 2023;13:175. doi: 10.1038/s41598-022-26314-8

[38] Oda Y, Shapiro MM, Lewis NM, et al. CsrA-controlled proteins reveal new dimensions of *Acinetobacter baumannii* desiccation tolerance. J Bacteriol. 2022;204(4):e0047921. doi: 10.1128/jb.00479-21

[39] Maharjan RP, Sullivan GJ, Adams FG, et al. DksA is a conserved master regulator of stress response in *Acinetobacter baumannii*. Nucleic Acids Res. 2023;51(12):6101–6119. doi: 10.1093/nar/gkad341

[40] Zhang Z, Chen C, Yang F, et al. Itaconate is a lysosomal inducer that promotes antibacterial innate immunity. Mol Cell. 2022;82(15):2844–2857.e10. doi: 10.1016/j.molcel.2022.05.009

[41] Chen M, Sun H, Boot M, et al. Itaconate is an effector of a Rab GTPase cell-autonomous host defense pathway against *Salmonella*. Science. 2020;369:450–455. doi: 10.1126/science.aaz1333

[42] Sambrook EF, Fritsch EF, Maniatis T. Molecular cloning: a laboratory manual. 1989.

[43] Lucidi M, Visaggio D, Prencipe E, et al. New shuttle vectors for real-time gene expression analysis in multidrug-resistant *Acinetobacter* species: *in vitro* and *in vivo* responses to environmental stressors. Appl Environ Microbiol. 2019;85(18):e01334–19. doi: 10.1128/AEM.01334-19

[44] Carpenter AE, Jones TR, Lamprecht MR, et al. CellProfiler: image analysis software for identifying and quantifying cell phenotypes. Genome Biol. 2006;7(10):R100. doi: 10.1186/gb-2006-7-10-r100

[45] Lucidi M, Runci F, Rampioni G, et al. New shuttle vectors for gene cloning and expression in multidrug-resistant *Acinetobacter* species. Antimicrob Agents Chemother. 2018;62:e02480–17. doi: 10.1128/AAC.02480-17

[46] Bashiri S, Lucidi M, Visaggio D, et al. Growth phase- and desiccation-dependent *Acinetobacter baumannii* morphology: an atomic force microscopy investigation. Langmuir. 2021;37:1110–1119. doi: 10.1021/acs.langmuir.0c02980

[47] Nečas D, Klapetek P. Gwyddion: an open-source software for SPM data analysis. Open Phys. 2012;10:181–188. doi: 10.2478/s11534-011-0096-2

[48] Eruslanov E, Kusmartsev S. Identification of ROS using oxidized DCFDA and flow-cytometry. Methods Mol Biol. 2010;594:57–72. doi: 10.1007/978-1-60761-411-1_4

[49] Runci F, Bonchi C, Frangipani E, et al. *Acinetobacter baumannii* biofilm formation in human serum and disruption by gallium. Antimicrob Agents Chemother. 2017;61(1):e01563–16. doi: 10.1128/AAC.01563-16

[50] Visaggio D, Pirolo M, Frangipani E, et al. A highly sensitive luminescent biosensor for the microvolumetric detection of the *Pseudomonas aeruginosa* siderophore pyochelin. ACS Sens. 2021;6(9):3273–3283. doi: 10.1021/acssensors.1c01023

[51] Antunes LCS, Imperi F, Carattoli A, et al. Deciphering the multifactorial nature of *Acinetobacter baumannii* pathogenicity. PLOS ONE. 2011;6:e22674. doi: 10.1371/journal.pone.0022674

[52] Runci F, Gentile V, Frangipani E, et al. Contribution of active iron uptake to *Acinetobacter baumannii* pathogenicity. Infect Immun. 2019;87:e00755–18. doi: 10.1128/IAI.00755-18

[53] Letizia M, Mellini M, Fortuna A, et al. PqsE expands and differentially modulates the RhlR quorum sensing regulon in *Pseudomonas aeruginosa*. Microbiol Spectr. 2022;10(3):e0096122. doi: 10.1128/spectrum.00961-22

[54] Huerta-Cepas J, Szklarczyk D, Heller D, et al. eggNOG 5.0: a hierarchical, functionally and phylogenetically annotated orthology resource based on 5090 organisms and 2502 viruses. Nucleic Acids Res. 2019;47:D309–14. doi: 10.1093/nar/gky1085

[55] Galperin MY, Kristensen DM, Makarova KS, et al. Microbial genome analysis: the COG approach. Brief Bioinform. 2019;20:1063–1070. doi: 10.1093/bib/bbx117

[56] Kanehisa M, Sato Y, Kawashima M. KEGG mapping tools for uncovering hidden features in biological data. Protein Sci. 2022;31(1):47–53. doi: 10.1002/pro.4172

[57] Wu T, Hu E, Xu S, et al. clusterProfiler 4.0: a universal enrichment tool for interpreting omics data. Innovation (Camb). 2021;2:100141. doi: 10.1016/j.xinn.2021.100141

[58] Aranda J, Poza M, Pardo BG, et al. A rapid and simple method for constructing stable mutants of *Acinetobacter baumannii*. BMC Microbiol. 2010;10(1):279. doi: 10.1186/1471-2180-10-279

[59] Heeb S, Itoh Y, Nishijyo T, et al. Small, stable shuttle vectors based on the minimal pVS1 replicon for use in gram-negative, plant-associated bacteria. Mol Plant Microbe Interact. 2000;13:232–237. doi: 10.1094/MPMI.2000.13.2.232